Journal of Renewable and Sustainable Energy

# Assessing intermittency characteristics via cumulant analysis of floating wind turbines wakes

Cite as: J. Renewable Sustainable Energy **13**, 013302 (2021); https://doi.org/10.1063/5.0022699
Submitted: 23 July 2020 . Accepted: 16 November 2020 . Published Online: 08 February 2021

Hawwa Kadum, Stanislav Rockel, Bianca Viggiano, Tamara Dib, Michael Hölling, Laurent Chevillard, and Raúl Bayoán Cal

Journal of Renewable and Sustainable Energy ARTICLE scitation.org/journal/rse

# Assessing intermittency characteristics via cumulant analysis of floating wind turbines wakes

Cite as: J. Renewable Sustainable Energy **13**, 013302 (2021); doi: 10.1063/5.0022699
Submitted: 23 July 2020 · Accepted: 16 November 2020 ·
Published Online: 8 February 2021

View Online Export Citation CrossMark

Hawwa Kadum,[1] Stanislav Rockel,[2] Bianca Viggiano,[1] Tamara Dib,[1] Michael Hölling,[2] Laurent Chevillard,[3] and Raúl Bayoán Cal[1,a)]

## AFFILIATIONS

[1]Department of Mechanical and Materials Engineering, Portland State University, Portland, Oregon 97201, USA
[2]ForWind, Institute of Physics, University of Oldenburg, Carl-von-Ossietzky-Str. 9-11, 26129 Oldenburg, Germany
[3]Univ. Lyon, ENS de Lyon, Univ. Claude Bernard, CNRS, Laboratoire de Physique, 46 allée d'Italie F-69342 Lyon, France

[a)]Author to whom correspondence should be addressed: rcal@pdx.edu

## ABSTRACT

Turbulence intermittency in the wake behind a single floating wind turbine as well as merging wakes due to a pair of floating turbines is investigated using magnitude cumulant analysis and non-analytical cumulant analysis. This low-order statistical approach is used to compute the intermittency for its impact on fatigue loading and power output signals. In the near wake, a 60% increase in the intermittency coefficient compared to the inflow is found. Pitch motion causes a 17% increase in intermittency compared to fixed turbines. The pitch-induced intermittency depletes in the far-wake, and hence, investigating whether a pitch-induced intermittency of one turbine affects a successive one in a wind array setting is recommended. Non-local scale interactions near rotor tips are observed as undulations in the cumulant profiles, referred to as tip-effect fluctuations. The impact of turbulence intensity on intermittency is also examined, and a positive correlation between the two is found in the near-wake. In the far-wake, however, it is found to speed up the pitch-induced intermittency depletion. The wake merging region between two neighboring turbines experiences lower intermittency and damps tip-effect fluctuations. This work provides more reliable intermittency estimation by utilizing lower moment statistics. The findings aid description, turbulent loading quantification, and stochastic modeling for floating wind farm wakes as well as fixed ones for both single and merging wakes.



## I. INTRODUCTION

Floating wind farms offer the ability to exploit vast ocean areas and propose a solution to land availability problems encountered when designing on-land farms. These ocean sites enjoy higher and more stable wind speeds, making the turbines more efficient than on land.[1,2] Wind turbines are typically designed to operate with a lifespan of 20 years, but on many occasions, they fail earlier than expected. One cause for the downtime is underestimated fatigue loads, leading to both reduced turbine performance and increased maintenance cost. The dynamic loading on turbines is directly related to the incoming flow turbulence characteristics.[3,4] Highly intermittent inflow results in intense torque fluctuations and intermittent output power signals. As floating wind turbines experience unique aerodynamics by undergoing pitch, surge, sway, heave, yaw, and roll motions,[5] it becomes necessary to investigate the effects produced by these motions on the turbine wake, in general,[6] and flow intermittency, in particular, given the difficulties with offshore maintenance. Due to scarcity of studies describing merging wakes, especially in offshore wind farms, it is of interest to investigate the intermittency in the region between two rotating turbines.

The interest in turbulence intermittency dates back to the description posed by Kolmogorov of scaling behavior of velocity increment moments as

$$B(\tau)^q = \langle \delta v_\tau^q \rangle \sim \tau^{\xi_q}. \quad (1)$$

$B(\tau)^q$ is the $q$th order structure function of time scales $\tau$, angular brackets denote time averaging, $\delta v_\tau$ is the velocity difference between two points that are separated by a time scale $\tau$, and $\xi$ is the scaling exponent.[7] The exponent $\xi$ has been found to be a non-linear function of the moments.[8–11] A modified model was proposed by Benzi *et al.*,[12] extended self-similarity model (ESS), in which the scaling exponent $\xi$ is a function of a $q$-independent function $f(\tau)$. Using this model, a

linear relationship is achieved for $\log(B(q_1,\tau))$ vs $\log(B(q_2,\tau))$.[13] However, in his model, the absolute values of velocity increments $|\delta v_\tau|^q$ are used.[12]

Castaing described the turbulence cascade and ESS accounting for the deformation in the probability distribution function[14–16] of velocity increments and time scales using the below equation:[17–20]

$$P_\tau(\delta v) = \int_{-\infty}^{\infty} G_{\tau\tau'}(u) e^{-u} P_{\tau'}(e^{-u}\delta v)\, du, \tag{2}$$

where $G_{\tau'}$ is a propagator and $\tau'$ is an arbitrary time scale that is larger than $\tau$. The velocity increments are decomposed as $\prod_{i=1}^{n} W_{\tau_{i+1},\tau'}\delta v_{\tau'}$, in which $W_{\tau_{i+1},\tau'}$ represents an independent variable of law $G_{\tau\tau'}$. The scaling exponent $\xi_q$ and the scale function $f(\tau)$ in the ESS approach can be related through the shape of $G_{\tau\tau'}$ via the "magnitude" of the cumulant generating function $\log|\delta v_\tau|$,[17]

$$\log \widehat{G_{\tau\tau'}}(-iq) = \log(B(q,\tau))/\log(B(q,\tau')) = \xi_q(f(\tau) - f(\tau')). \tag{3}$$

The estimation of structure functions for higher orders can be challenging when seeking statistical convergence. Delour *et al.*[17] suggested an alternative approach in which the intermittency coefficient can be estimated without computing moments as high as the $6^{th}$ order using the former relation between the velocity increment and the propagator $G_{\tau\tau'}$. In this approach, the magnitude cumulant analysis, the polynomial development of $\log(B(q,\tau))/\log(B(q,\tau'))$ vs $q$ includes the cumulants $C_n(\tau) = -c_n f(\tau)$ of the generator $\log|\delta v_\tau|$ and the cumulants are given by[21]

$$\langle|\delta v_\tau|^q\rangle = \exp\left(\sum_{n=1}^{+\infty} C_n(\tau)\frac{q^n}{n!}\right), \tag{4}$$

where the first, second, and third cumulants are described as

$$C_1(\tau) = \langle \log|\delta v_\tau|\rangle \quad \sim -c_1 \log(\tau), \tag{5}$$

$$C_2(\tau) = \langle \log|\delta v_\tau|^2\rangle - \langle \log|\delta v_\tau|\rangle^2 \quad \sim -c_2 \log(\tau), \tag{6}$$

$$C_3(\tau) = \langle \log|\delta v_\tau|^3\rangle - 3\langle \log|\delta v_\tau|^2\rangle\langle \log|\delta v_\tau|\rangle + 2\langle \log|\delta v_\tau|\rangle^3 \quad \sim -c_3 \log(\tau). \tag{7}$$

Typically, the 6th order structure function is used to obtain intermittency exponent $\mu = 2 - \xi_6$ for long-normal processes.[22,23] Basu *et al.*[21] state that a relation between the intermittency exponent $\mu$ and the second cumulant coefficient $c_2$ for a log-normal process can be arrived by relating velocity increments to the coarse grained dissipation rate that scales as $\tau^{-M_q}$ using the formula $\xi_q = q/3 - M_{q/3}$, where $M_2 = \mu$. Using Eq. (4) for the second cumulant, one arrives at $M_q = (-\mu/18)\log\tau$, while for a lognormal process, $M_q = \mu(q^2 - q)/2$. Hence, the relation between the intermittency exponent and the second cumulant coefficient is described as

$$\mu = 9c_2. \tag{8}$$

Thus, the intermittency exponent can be obtained without resorting to the 6th moment statistics by employing the magnitude cumulant analysis.

For a Gaussian process, the asymptotic values of the three cumulants at large scales ($\tau \to T$) are $C_1(\tau) = -0.64$, $C_2(\tau) = \pi^2/8$, and $C_3(\tau) = -2.1$ where $T$ is the integral time scale.[21] Previous studies also show that the third cumulant has a slope of zero.[21,24]

Cumulant analysis, both magnitude and non-analytical approaches, is herein used to describe and quantify the turbulence intermittency in the wakes of floating wind turbines. This approach enables the determination of intermittency caused by pitch motion by comparing it to a fixed wind turbine. Furthermore, the turbulence intermittency behavior of the flow between two oscillating wind turbines is investigated. Cumulant analysis captures the flow intermittency without the computation of higher order statistics such as structure functions, thus overcoming the statistical convergence problem. Offshore wind turbines endure higher fatigue loads due to the complicated dynamics they experience due to wave-turbine and wind-turbine interactions. Those interactions apply cyclic loads on the turbines, pitch, surge, and sway motions, to name a few. Comprehending the wake flow of an oscillating wind turbine advances the design and power production optimization of offshore wind farms. Moreover, more reliable estimations of intermittency reduce the turbine downtime and maintenance related to dynamic load underestimation. The analysis conducted in this study describes the turbulence cascade of those wakes and quantifies its intermittency.

## II. DATA DESCRIPTION

The data are collected in two closed loop wind tunnels at the University of Oldenburg. Each wind tunnel has a test section with a cross-sectional area of 0.8 m × 1 m, but differ in length. One wind tunnel has a 2.6 m long test section, while the other has a 5 m long test section. The test section is equipped with a grid located at its entrance. The grid consists of winglets attached to seven horizontal and nine vertical shafts. The shafts are then connected to motors that can be set to run according to prescribed protocols to generate a desired turbulence intensity of the incoming flow.[25]

The turbine model consists of a rotor diameter of 0.2 m, a diameter of 0.028 m and a long nacelle of 0.24 m, and a diameter motor of 0.016 m. The data are collected using 1 mm length Dantec 55*P*16 hot-wires that are operated using a *CTA* 54*N*80 Dantec multichannel.[25]

Two sets of experimental data have been used in the analysis: single floating and fixed wind turbine conducted in the 2.6 m long test section wind tunnel and two floating and fixed wind turbines conducted in the 5 m long test section wind tunnel. The experimental setup of each dataset is described below.

### A. Single wind turbine

A single wind turbine model free to oscillate in the streamwise direction with a pitch angle up to 15° is used. The oscillations are caused by the incoming wind. The turbine is placed 1.09 m from the entrance, and the data are collected at downstream locations up to 7*D*. A total of 16 hot-wires are placed on a rake to collect the data in eight vertical, four horizontal, and four in 45° diagonal locations with a spacing of 33 mm (0.165*D*)between each two successive hot-wires, see Fig. 1. The turbine is subjected to two inflow conditions: (1) passive grid case in which the grid is fixed and a low turbulence intensity of 1.8% is produced and (2) active grid case in the grid is ran through variable speed protocol and a high turbulence intensity of 15.9% is generated. The same tests are performed on a fixed wind turbine for comparison. A detailed description of this dataset can be found in Refs. 26, 27, and the experimental setup schematic is presented in Fig. 1, where *TT*, *ATT*, *HH*, and *BT* are acronyms for the top tip, above

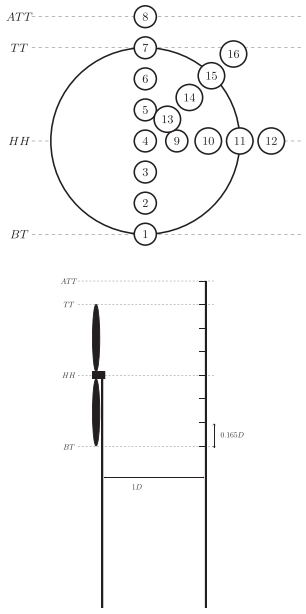


FIG. 1. Single wind turbine model and measurement locations (bottom). Front view of hot-wires rake (top).

top tip, hub height, and bottom tip locations. A summary of the different experimental cases studied is shown in Table I.

### B. Two wind turbines

The second data set used in this study is for two floating wind turbines oscillating concurrently.[28] The turbines are placed next to each other horizontally facing a passive grid inflow condition with a turbulence intensity of 4%. The measurements are collected 1$D$, 3$D$, and 5$D$ behind the two turbines at the hub height using 11 one-dimensional hot-wires at a sampling frequency of 20 kHz. The hot-wires are spaced 7.5 cm (0.375$D$) in the spanwise direction except for the hot-wires in between the two turbines that are 5 cm (0.25$D$) apart. A top view of the setting is illustrated in Fig. 2. A summary of the different experimental cases studied is shown in Table I.

## III. RESULTS

### A. Method validation and inflow characterization

To validate the methods used to compute the cumulants and the experimental measurements, magnitude cumulants are shown for direct

TABLE I. Cases studied. TI is the inflow turbulence intensity.

| Single wind turbine | Turbine type | Grid | TI |
|---|---|---|---|
| | Fixed | Passive | 1.8% |
| | Fixed | Active | 15.9% |
| | Floating | Passive | 1.8% |
| | Floating | Active | 15.9% |
| Two wind turbines | Turbine type | Grid | TI |
| | Floating | Passive | 4% |

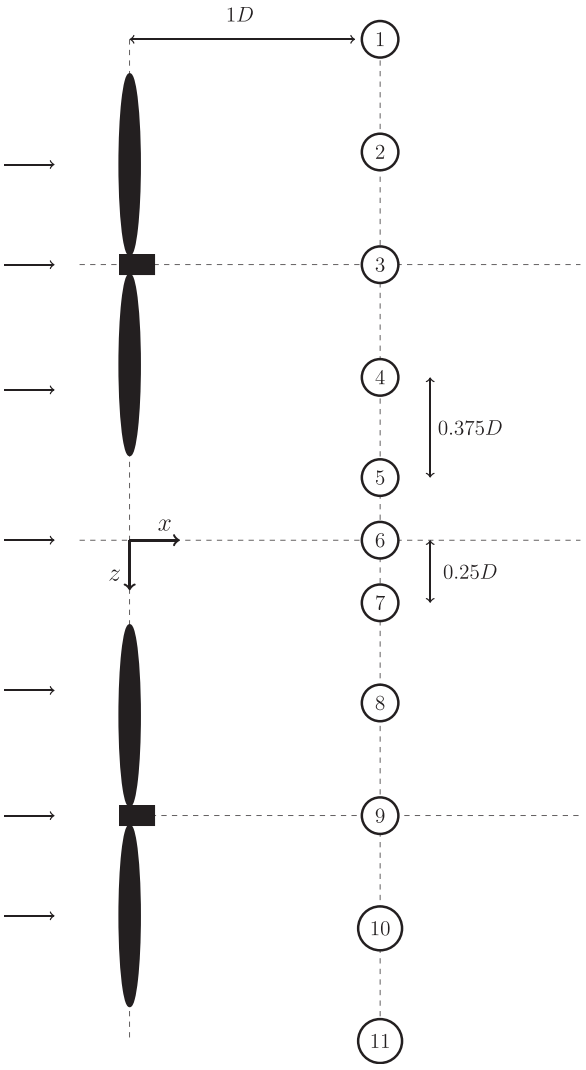


FIG. 2. Two wind turbine setups and measurement locations. Measurements are taken at the hub height).

numerical simulations (DNSs) of homogeneous isotropic turbulence. This data set is used herein as it has been shown in previous studies[24] that the second cumulant typically displays three scaling regions: far dissipation range, near dissipation range, and inertial subrange. The inertial range was shown to follow a slope of $-c_2 = -0.025$. The same region follows a slope of $c_1 = 1/3 + 3c_2/2$ in the first cumulant profile, while the far dissipation range exhibits a $-1$ slope. Figure 3 presents the first and second order magnitude cumulants for the DNS data. The vertical axis in the second cumulant represents $C_2(\tau) - (\pi^2/8)$, but referred to as $C_2(\tau)$ throughout this paper for simplicity. The second order coefficient $c_2$ is referred to as an intermittency coefficient for herein. The figure shows the regions described earlier,[24] confirming the accuracy of the method for computations.

The methods are applied to characterize the inflow of the experimental data set used in this work. Figure 4 presents the cumulants for

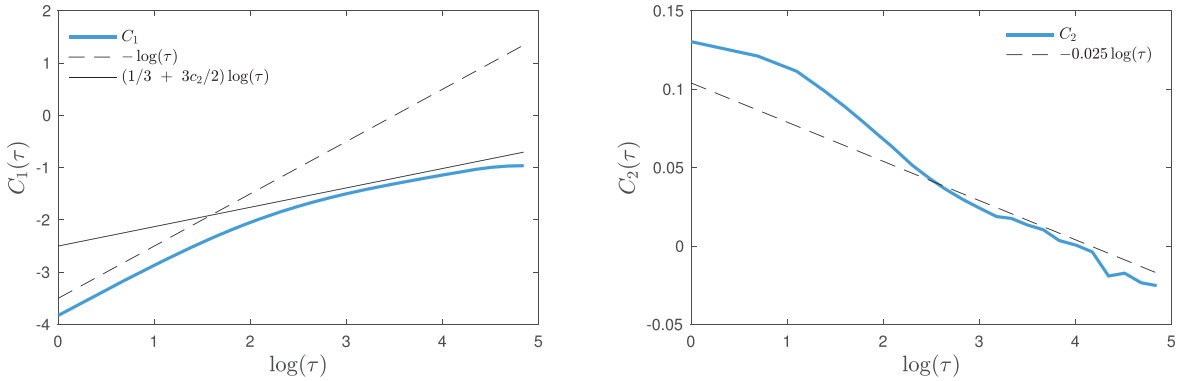


**FIG. 3.** First and second order cumulants of a DNS dataset for the isotropic flow field.

the two inflow conditions generated using active and passive grid arrangements. The cumulants at each time scale $\tau$ are plotted against the time scales normalized by the separation time scale $\tau_s$, the scale at which the inertial range ends and the second cumulant asymptotes. Two vertical dashed lines are used to indicate the inertial subrange over which the cumulant slopes are obtained. Each case has its own scaling range that is obtained from the region that follows the $(1/3 + 3c_2/2)\log(\tau/\tau_s)$ law in the first cumulant profile. This method has been used in previous studies that conducted magnitude cumulant analysis. However, the cumulant method was checked against the traditional energy spectra method[29,30] for further confirmation. The scaling regions determined using both methods yielded similar results (not shown) with lower uncertainty in the cumulant approach results. Hence, the latter method will be used herein. The inflow exhibits typical cumulant profiles, and the inertial range is identified. The inertial range has intermittency coefficients of $c_2 = 0.023$ and $c_2 = 0.026$ in the passive and active grid flow, respectively, and the first cumulant coincides with $c_1 = 1/3 + 3c_2/2$ in that region. Referring to Eq. (1), the intermittency exponent $\mu$ for passive and active grid inflow is 0.2 and 0.23, respectively. These values fall within the range of $\mu = 0.25 \pm 0.05$ estimated by Sreenivasan *et al.*[31,32]

## B. Turbine type and turbulence intensity

To assess the effect of pitch motion on flow intermittency, Fig. 5 presents the first and second cumulants of a floating wind turbine compared to a fixed wind turbine. The pitch motion effects have been found to be more apparent in flows with lower turbulence intensity,[33] and hence, the passive grid case is presented in Fig. 5. The figure shows that interaction with the wind turbine increases flow intermittency in the near wake. The intermittency coefficients are $c_2 = 0.041$ and $c_2 = 0.048$ for the fixed and floating wind turbines, respectively. These values are at least 60% higher than ≈0.025 in the inflow. The results also suggest pitch motion increasing the intermittency by about 17% at that location compared to the fixed wind turbine.

The impact of inflow turbulence intensity on floating wind turbine intermittency is presented in Fig. 6. The figure shows an increase of 14% in intermittency when the inflow turbulence intensity of the inflow increased from 1.8% to 15.9%. The structure of a wind turbine in a floating wind farm setting, hence, endures more dynamic loads caused by the turbine oscillations that increase with increased flow turbulence intensity. It is then necessary to account for the additional intermittency when modeling a floating wind turbine wake and when predicting its lifespan.

## C. Vertical location dependence

The results presented above correspond to the bottom tip location. However, it is recognized that the wake generated by the wind turbine varies significantly depending on the location along the turbine height. The top tip location is associated with complex aerodynamics,

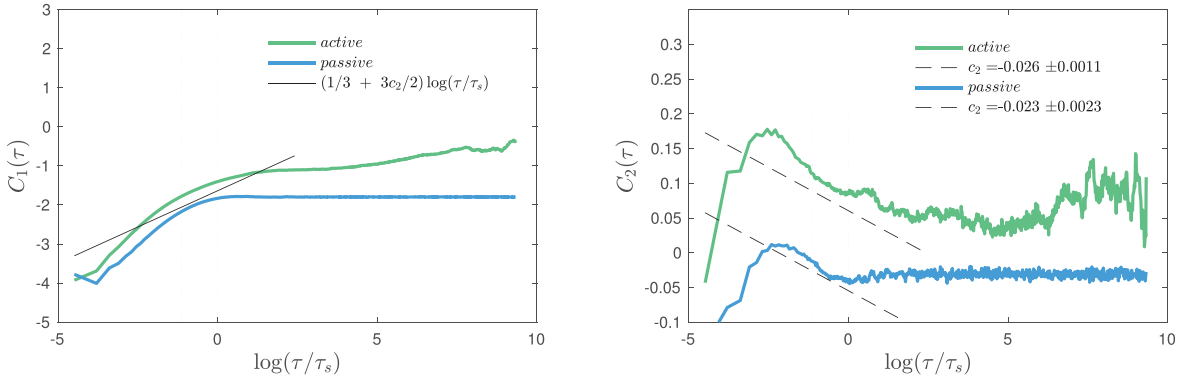


**FIG. 4.** First and second order cumulants for the inflow generated using passive and active grids.

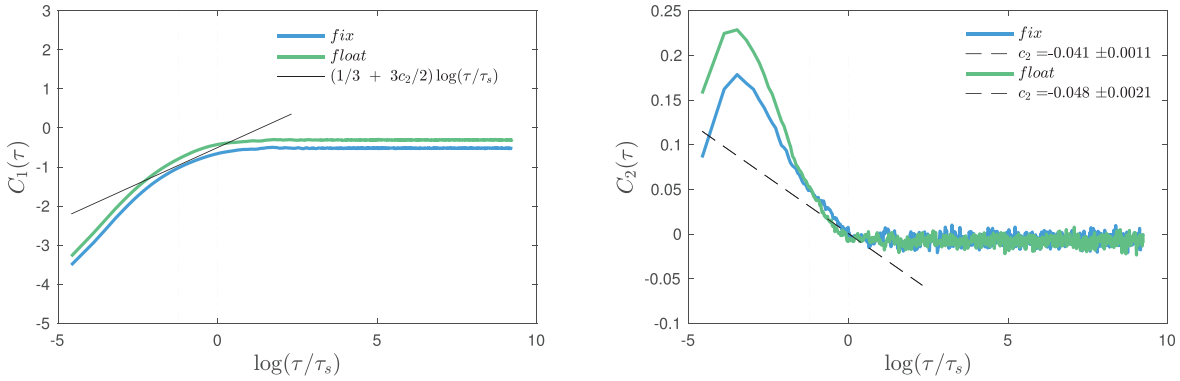


**FIG. 5.** First and second order cumulants for a fixed and floating wind turbine in the passive grid condition. The cumulant is computed 1*D* downstream the bottom tip location.

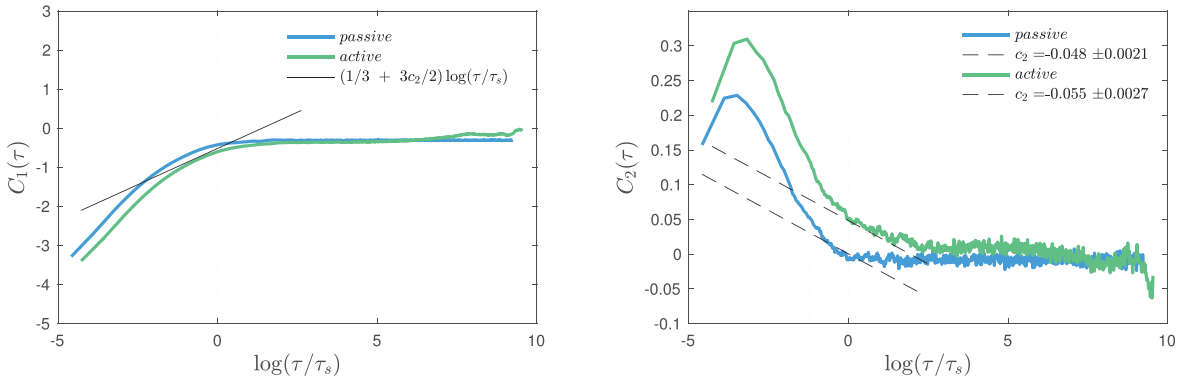


**FIG. 6.** First and second order cumulants 1*D* downstream the bottom tip of a floating wind turbine under passive and active inflow conditions.

and thus, Fig. 7 demonstrates the cumulants at this location in the near wake. The second cumulant profile does not accurately identify the inertial range as the profile does not coincide with a slope close to $-0.025$, and no region in the first cumulant profile aligns with $c_1 = 1/3 + 3c_2/2$. The profiles exhibit high-intensity undulations after the dissipation range, making it challenging to detect the inertial range. The undulations are existent in both turbine types and believed to be caused by flow dynamics associated with the rotor tip location like tip vortex shedding. These undulations will be referred to as tip-effect fluctuations hereon. The tip-effect fluctuations suggest non-local scale interactions that lead to perturbations in the scaling cascade as observed in the top tip cumulant profiles. Tip-effect fluctuations do

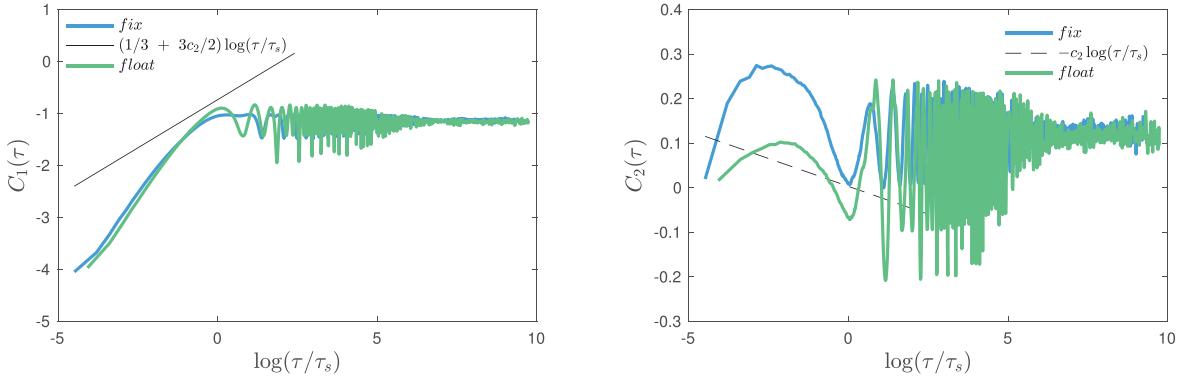


**FIG. 7.** First and second order cumulants 1*D* downstream the top tip of a floating and a fixed wind turbine under passive inflow conditions.

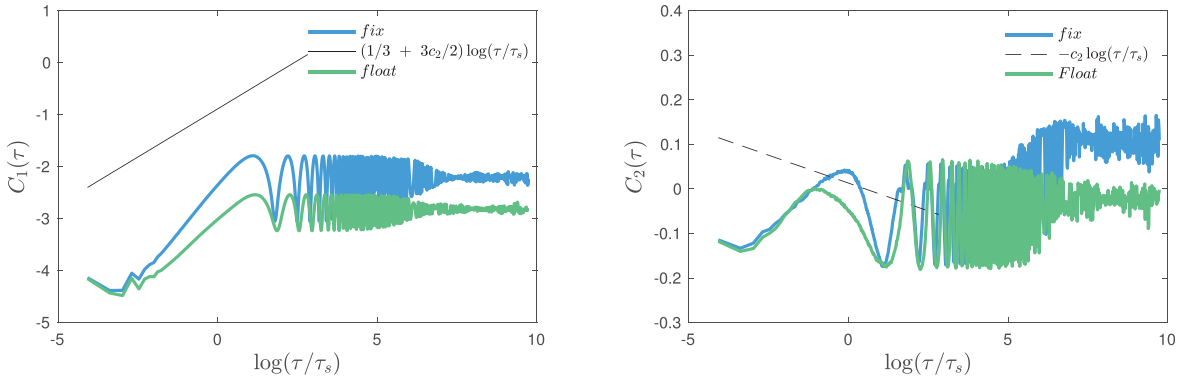


**FIG. 8.** First and second order cumulants 1*D* downstream the location 0.165*D* above the top tip of a floating and a fixed wind turbine under passive inflow conditions.

not exist at the bottom tip location due to the turbine nacelle blocking the flow preventing any non-local scale interactions from occurring.

The floating wind turbine profiles display additional fluctuations, and hence, they are caused by the pitch motion. Similar behavior is observed in the flow immediately above the top tip location, see Fig. 8. These results suggest that the intermittency in those specific locations is hard to quantify using cumulant analysis or any scaling-dependent approach. Whether this conclusion is true for other downstream locations is investigated in subsection III D. Nevertheless, it is recommended to use alternative techniques to evaluate intermittency in near rotor tip locations like Hilbert–Huang analysis.[33]

### D. Downstream development

The results so far concern the flow near the wake, specifically 1*D* downstream the turbines. The intermittency development up to 7*D* downstream is examined herein. Figure 9 presents the first and second cumulants of a floating wind turbine in a passive grid inflow condition. The cumulants are obtained for wake flow 1*D*, 3*D*, 5*D*, and 7*D* behind the top tip. The inertial range is not identified even at 3*D* downstream the rotor due to tip-effect fluctuations in the profiles propagating further downstream. At 5*D*, these fluctuations diminish, and the inertial range is apparent. The intermittency at 5*D* is 28% higher than the inflow with $c_2 = 0.032$, and the intermittency added to the flow due to interaction with the turbine persists up until 7*D* behind the turbine where $c_2 = 0.025$. The intermittency caused by tip-effect fluctuations, and flow-turbine interaction, in general, dissipates gradually before vanishing seven rotor diameters downstream the turbine.

In Fig. 10, the downstream development of cumulants and intermittency for a floating wind turbine in an active grid inflow arrangement is presented. The figure highlights an interesting finding of higher turbulence intensity flow. Although the active grid case resulted in higher intermittency than the passive grid at 1*D*, Fig. 10 shows that the active grid leads to faster recovery of the flow in terms of tip-effect fluctuations caused by tip vortex shedding and pitch motion. The inertial range is identified at 5*D* downstream of the turbine in the passive grid case, whereas in the active grid case, the range is clearly observed at 3*D*. Furthermore, the intermittency level at this location is equal to the intermittency level of the passive grid case at 5*D* where their intermittency coefficients are $-c_2 = -0.033$ and $-c_2 = -0.032$, respectively, meaning that the higher turbulence intensity can break any flow structures caused by the pitch motion faster, generating a flow with a linear turbulence scale cascade in the inertial subrange.

The downstream development of intermittency for a fixed wind turbine is examined in Fig. 11. Similar to a floating wind turbine, the inertial range scaling is recovered 3*D* downstream of the rotor in an

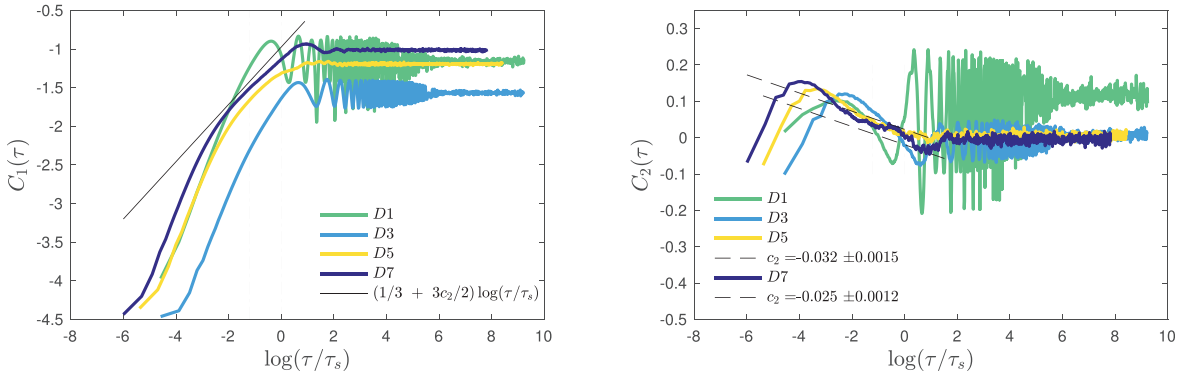


**FIG. 9.** Downstream development of cumulants at the top tip of a floating wind turbine under passive grid inflow conditions.

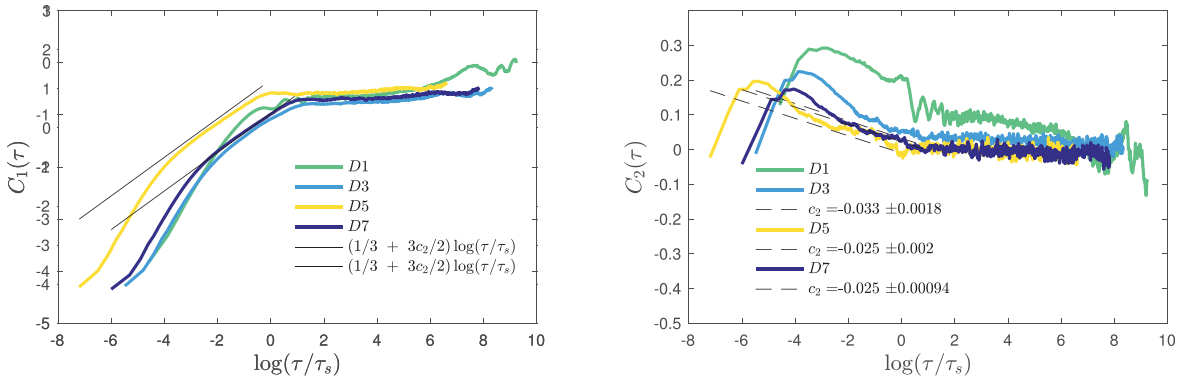


**FIG. 10.** Downstream development of cumulants at the top tip of a floating wind turbine under active grid inflow conditions.

active grid inflow condition. The difference in intermittency between floating and fixed wind turbines found at 1$D$ downstream the rotor is marginal at 3$D$, where the aforementioned turbines have intermittency coefficients of $-c_2 = -0.032$ and $-c_2 = -0.03$, respectively.

### E. Two merging wakes

Here, the flow intermittency 1$D$ downstream merging wakes generated by two aligned turbines is examined. Figure 12 shows the second cumulant at selected locations illustrated in the schematic provided on the right side of the figure. Points located near the rotor tips, $P_1$ and $P_{11}$, experience the tip-effect fluctuations observed in the top tip and above the top tip locations in the single wind turbine wake. The inertial range is, thus, hard to identify, the intermittency coefficient cannot be accurately obtained, and the inertial subrange is also not observed in the first cumulant profile (not shown). It is noted that location $P_1$ experiences lower tip-effect fluctuations than location $P_{11}$ even though they are equally distanced from the rotor tips, suggesting dependency on the turbine rotation direction. The locations to the positive side of the rotation direction $(+z)$ undergo higher rotor tip effects compared to the points on the $(-z)$ side. Location $P_9$ behind the rotor hub exhibits a typical second cumulant trend with an intermittency coefficient of $c_2 = 0.025$. The wakes merging locations $P_5$, $P_6$, and $P_7$ are presented in the lower three subfigures. Locations $P_5$ and $P_7$ are near rotor tips; however, unlike in locations $P_1$ and $P_{11}$, the tip-effect fluctuations do not appear in their profiles.

This observation is evidence of damping happening when two wakes meet. In addition to damping the tip-effect fluctuations, the intermittency is also lowered compared to the near wake of a single wind turbine. For a bottom tip location 1$D$ behind a single wind turbine, the second cumulant coefficient is $c_2 = 0.048$ for a flow with a 1.8% turbulence intensity. For a flow with a 4% turbulence intensity near rotor tip locations at $P_5$ and $P_7$, the second cumulant coefficients for two merging wakes are $c_2 = 0.023$ and $c_2 = 0.033$, respectively. Merging wakes reduce extreme events in the wake flow helping wind farms reduce intermittency compared to a single wind turbine. This is even more evident at the center of merging wakes, represented by location $P_6$ in Fig. 12. Location $P_6$ has a negligible second order coefficient of $c_2 = 0.0068$, which is an order of magnitude lower than other locations. The aforementioned findings are an advantage for staggered wind farms where the turbines of one row are located in the wake-merging regions of a previous row.

## IV. CONCLUSIONS

The current study examines intermittency in wind turbines experiencing pitch motion using magnitude cumulant analysis. The results show the inflow possessing a typical second cumulant coefficient of $c_2 \approx 0.025$. When the flow interacts with the turbine, an increase of at

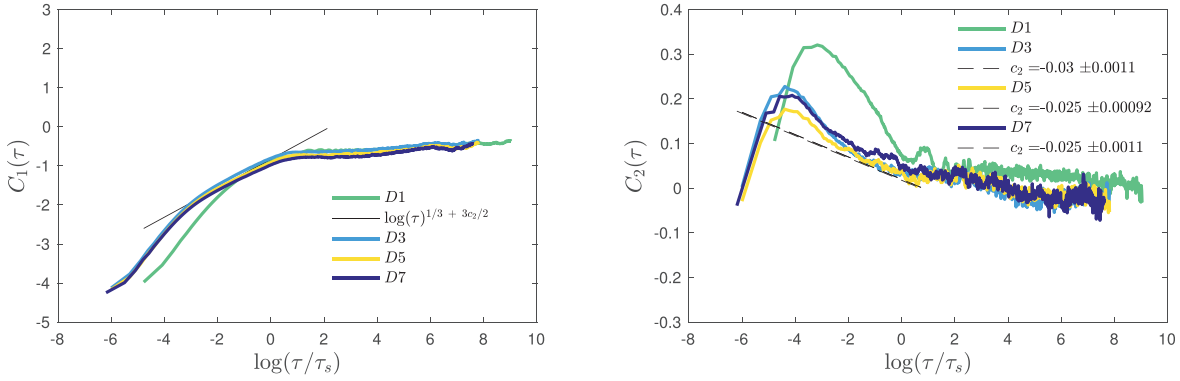


**FIG. 11.** Downstream development of cumulants at the top tip of a fixed wind turbine under active grid inflow conditions.

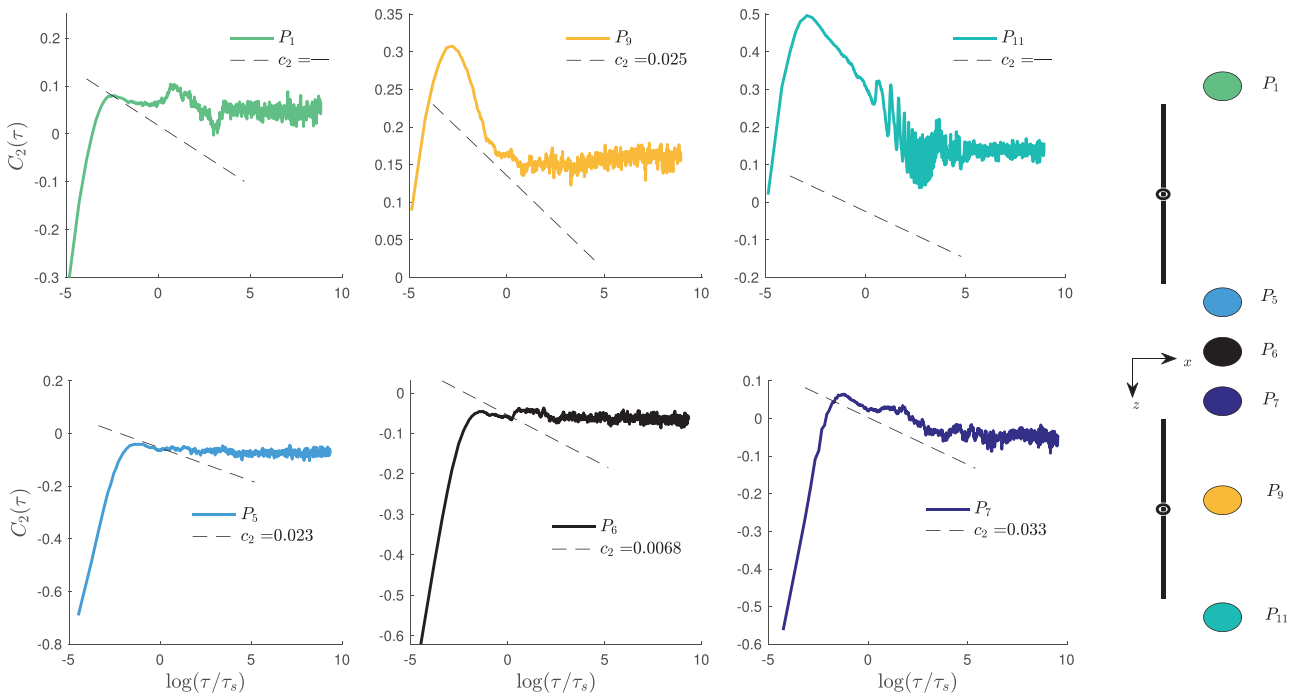


**FIG. 12.** Second order cumulants at various spanwise locations 1*D* behind two floating wind turbines under passive grid inflow conditions.

least 60% from that value is found 1*D* downstream of the rotor. The pitch motion results in 17% higher intermittency in the floating wind turbine compared to the fixed wind turbine. This study also reports an increase in the intermittency coefficient of 14% when the inflow turbulence intensity is increased by 78%.

Non-local scale interactions are observed near the rotor tips, except the bottom tip. These interactions cause tip-effect fluctuations in the cumulant profiles. The pitch motion is found to cause additional fluctuations that are only found in the floating wind turbine wake. The tip-effect fluctuations lead to difficulties in identifying the inertial subrange, and hence, the intermittency is not obtained for those locations in the near-wake flow.

For the passive grid inflow condition, the tip-effect fluctuations travel up until 5*D* downstream of the rotor. Interestingly, higher turbulence intensity is found to speed up the dissipation of tip-effect fluctuations. For that active grid case, these fluctuations travel only 3*D* downstream. Furthermore, after 3*D*, the active grid flow no longer causes higher intermittency than the passive grid as both cases are found to have equal intermittency coefficients of $c_2 \approx 0.033$. The same is true for the pitch motion. Floating and fixed wind turbines have equal intermittency coefficients after 3*D* downstream. The latter observation suggests that the intermittency caused by pitch motion of a single turbine does not impact turbines in a successive row, although the pitch motion of each turbine still impacts the same turbine. This behavior needs to be further tested in a wind turbine array setting.

In a floating wind farm setup, the tip-effect fluctuations are diminished in the wake merging region between two neighboring turbines. This region demonstrates a reduced level of intermittency compared to similar locations with a single wake flow. The center of the merging region reported a one order of magnitude lower intermittency coefficient.

## ACKNOWLEDGMENTS

The authors would like to acknowledge the valuable comments and fruitful discussions withProfessor Joachim Peinke throughout this work.

## DATA AVAILABILITY

The data that support the findings of this study are available from the corresponding author upon request.

## REFERENCES

[1]N. Ali, N. Hamilton, M. Calaf, and R. B. Cal, Journal of Turbulence **20**(1), 32–63 (2019).
[2]R. Scott, B. Viggiano, T. Dib, N. Ali, M. Hölling, J. Peinke, and R. B. Cal, "Wind turbine partial wake merging description and quantification," Wind Energy **23**(7), 1610–1618 (2020).
[3]M. Khosravi, P. Sarkar, and H. Hu, J. Phys.: Conf. Ser. **753**, 092015 (2016).
[4]R. B. Cal, J. Lebrón, L. Castillo, H. S. Kang, and C. Meneveau, J. Renewable Sustainable Energy **2**(1), 013106 (2010).
[5]R. Scott, J. Bossuyt, and R. B. Cal, J. Renewable Sustainable Energy **12**(4), 043302 (2020).
[6]S. Rockel, E. Camp, J. Schmidt, J. Peinke, R. Cal, and M. Hölling, Energies **7**, 1954 (2014).
[7]T. Mücke, D. Kleinhans, and J. Peinke, Wind Energy **14**, 301 (2011).
[8] N. Ali, H. F. Kadum, and R. B. Cal, J. Renewable Sustainable Energy **8**(6), 063306 (2016).
[9]U. Frisch, *Turbulence: The Legacy of A.N. Kolmogorov* (Cambridge University Press, 1995).

[10]A. S. Monin and A. M. Yaglom, *Statistical Fluid Mechanics, Volume II: Mechanics of Turbulence* (Courier Corporation, 2013).
[11]F. Anselmet, Y. Gagne, E. Hopfinger, and R. Antonia, J. Fluid Mech. **140**, 63 (1984).
[12]A. Arneodo, Europhys. Lett. **34**, 411 (1996).
[13]R. Benzi, S. Ciliberto, R. Tripiccione, C. Baudet, F. Massaioli, and S. Succi, Phys. Rev. E **48**, R29 (1993).
[14]M. S. Melius, M. Tutkun, and R. B. Cal, J. Renewable Sustainable Energy **6**(2), 023121 (2014).
[15]M. S. Melius, M. Tutkun, and R. B. Cal, Phys. D **280-281**, 14–21 (2014).
[16]B. Viggiano, M. S. Gion, N. Ali, M. Tutkun, and R. B. Cal, J. Renewable Sustainable Energy **8**(5), 053310 (2016).
[17]N. Ali, A. S. Aseyev, and R. B. Cal, J. Renewable Sustainable Energy **8**, 013304 (2016).
[18]J. Delour, J. Muzy, and A. Arneodo, Eur. Phys. J. B **23**, 243 (2001).
[19]B. Castaing, Y. Gagne, and E. Hopfinger, Phys. D **46**, 177 (1990).
[20]N. Ali and R. B. Cal, Chaos, Solitons & Fractals **119**, 215–229 (2019).
[21]B. Castaing, Y. Gagne, and M. Marchand, Phys. D **68**, 387 (1993).
[22]N. Ali, A. Fuchs, I. Neunaber, J. Peinke, and R. B. Cal, Journal of Turbulence **20**(2), 93–120 (2019).
[23]Y. Malécot, C. Auriault, H. Kahalerras, Y. Gagne, O. Chanal, B. Chabaud, and B. Castaing, Eur. Phys. J. B **16**, 549 (2000).
[24]S. Basu, E. Foufoula-Georgiou, B. Lashermes, and A. Arnéodo, Phys. Fluids **19**, 115102 (2007).
[25]S. Rockel, J. Peinke, M. Hölling, and R. B. Cal, Renewable Energy **85**, 666–676 (2016).
[26]L. Chevillard, B. Castaing, and E. Lévêque, Eur. Phys. J. B **45**, 561 (2005).
[27]S. Rockel, J. Peinke, M. Hölling, and R. B. Cal, Renewable Energy **112**, 1 (2017).
[28]I. Neunaber, M. Hölling, R. J. Stevens, G. Schepers, and J. Peinke, Energies **13**, 5392 (2020).
[29]D. G. Ortiz-Suslow, Q. Wang, J. Kalogiros, and R. Yamaguchi, J. Atmos. Oceanic Technol. **37**, 85 (2020).
[30]K. Sreenivasan and P. Kailasnath, Phys. Fluids A **5**, 512 (1993).
[31]K. R. Sreenivasan and R. Antonia, Annu. Rev. Fluid Mech. **29**, 435 (1997).
[32]H. Kadum, S. Rockel, M. Hölling, J. Peinke, and R. B. Cal, J. Renewable Sustainable Energy **11**, 053302 (2019).
[33]F. G. Schmitt, Y. Huang, Z. Lu, Y. Liu, and N. Fernandez, J. Mar. Syst. **77**, 473 (2009).